



This is a repository copy of *Clustering in gallium ion beam sputtered compound materials driven by bond strength and interstitial/vacancy reaction*.

White Rose Research Online URL for this paper:

<https://eprints.whiterose.ac.uk/215071/>

Version: Accepted Version

---

**Article:**

Ma, Z. [orcid.org/0000-0003-2508-6499](https://orcid.org/0000-0003-2508-6499), Zhang, X., Liu, P. et al. (13 more authors) (2023) Clustering in gallium ion beam sputtered compound materials driven by bond strength and interstitial/vacancy reaction. *Applied Physics Letters*, 123 (10). 102101. ISSN 0003-6951

<https://doi.org/10.1063/5.0161681>

---

© 2023 The Authors. Except as otherwise noted, this author-accepted version of a journal article published in *Applied Physics Letters* is made available via the University of Sheffield Research Publications and Copyright Policy under the terms of the Creative Commons Attribution 4.0 International License (CC-BY 4.0), which permits unrestricted use, distribution and reproduction in any medium, provided the original work is properly cited. To view a copy of this licence, visit <http://creativecommons.org/licenses/by/4.0/>

**Reuse**

This article is distributed under the terms of the Creative Commons Attribution (CC BY) licence. This licence allows you to distribute, remix, tweak, and build upon the work, even commercially, as long as you credit the authors for the original work. More information and the full terms of the licence here:

<https://creativecommons.org/licenses/>

**Takedown**

If you consider content in White Rose Research Online to be in breach of UK law, please notify us by emailing [eprints@whiterose.ac.uk](mailto:eprints@whiterose.ac.uk) including the URL of the record and the reason for the withdrawal request.



[eprints@whiterose.ac.uk](mailto:eprints@whiterose.ac.uk)  
<https://eprints.whiterose.ac.uk/>

This is the author's peer reviewed, accepted manuscript. However, the online version of record will be different from this version once it has been copyedited and typeset.

PLEASE CITE THIS ARTICLE AS DOI: 10.1063/5.0161681

## Clustering in gallium ion beam sputtered compound materials driven by bond strength and interstitial/vacancy reaction

Zhenyu Ma<sup>1,\*</sup>, Xin Zhang<sup>1,\*</sup>, Pu Liu<sup>2</sup>, Yong Deng<sup>1,3</sup>, Wenyu Hu<sup>3</sup>, Longqing Chen<sup>4</sup>, Jun Zhu<sup>5</sup>, Sen Chen<sup>6</sup>, Zhengshang Wang<sup>7</sup>, Yuechun Shi<sup>8</sup>, Jian Ma<sup>1</sup>, Xiaoyi Wang<sup>1,a)</sup>, Yang Qiu<sup>3,a)</sup>, Kun Zhang<sup>4</sup>, Xudong Cui<sup>9</sup>, Thomas Walther<sup>10</sup>

<sup>1</sup>Southwest Minzu University, State Ethnic Affairs Commission, Chengdu 610041, China

<sup>2</sup>NCS Testing Technology Co. LTD, Chengdu 610041, China

<sup>3</sup>Pico center, SUSTech Core Research Facilities, Southern University of Science and Technology, Shenzhen 518055, China

<sup>4</sup>Key Laboratory of Radiation Physics and Technology of Ministry of Education, Institute of Nuclear Science and Technology,

Sichuan University, Chengdu 610064, China

<sup>5</sup>College of Physical Science and Technology, Sichuan University, Chengdu 610064, China

<sup>6</sup>Laboratory for Shock Wave and Detonation Physics, Institute of Fluid Physics, China Academy of Engineering Physics,

Mianyang, Sichuan 621900, China

<sup>7</sup>Sichuan Research Center of New Materials, 596 Yinhe Road, Shuangliu, Chengdu 610200, China

<sup>8</sup>Yongjiang Laboratory, Ningbo 315000, China

<sup>9</sup>Institute of Chemical Materials, China Academy of Engineering Physics, Mianyang 621900, China

<sup>10</sup>Dept. Electronic & Electrical Eng., University of Sheffield, Mappin St., Sheffield S1 3JD, UK

\*Authors to whom correspondence should be addressed: [80300024@swun.edu.cn](mailto:80300024@swun.edu.cn) and [qiuy@sustech.edu.cn](mailto:qiuy@sustech.edu.cn)

(Date: 8 May 2023, in revised form 17/8/2023)

**Abstract:** The investigation of chemical reactions during ion irradiation is a frontier for the study of the ion-material interaction. In order to probe the chemistry of ion produced nanoclusters, valence electron energy loss spectroscopy (VEELS) was exploited to investigate Ga<sup>+</sup> ion damage in Al<sub>2</sub>O<sub>3</sub>, InP and InGaAs, where each target material has been shown to react differently to the interaction between impinging ions, recoil atoms and vacancies: metallic Ga, ternary InGaP clusters and metallic In clusters are formed in Al<sub>2</sub>O<sub>3</sub>, InP and InGaAs, respectively. Supporting simulations based on Monte Carlo and crystal orbital Hamiltonian calculations indicate that the chemical constitution of cascade induced nano-precipitates is a result of a competition between interstitial/vacancy consumption rates and preferential bond formation due to differing bond strengths.

An understanding of energetic particle induced physical or chemical alteration in compound materials has always been the subject of nuclear physics<sup>1-5</sup> and advanced material processing<sup>6-11</sup>. In the last decades, various mechanisms of ion beam irradiation damage have been predicted through density functional theory<sup>12-14</sup> and hybrid molecular dynamics/Monte Carlo (MD/MC) simulations<sup>15-19</sup>, including the production and recombination of Frenkel pairs<sup>20,21</sup>, cascade induced interstitial/vacancy clustering<sup>22,23</sup> and long-range glissile loop absorption<sup>24</sup>. These theories are of importance to describe the

projectile ion dynamics in bulk materials. In fact, contributions by chemical reactions have been totally ignored until Hofsärs and Zhang proposed the new concept of "surfactant sputtering"<sup>25-27</sup>. During ion beam sputtering, additional phases may be formed by chemical reactions between incident ions and target atoms, as well as between target atoms. This will have impact on the sputtering result, including changes in elemental sputtering rate, mass redistribution related to recoil atoms, local strain and phase separation, further altering the sputtering rate. The conventional techniques used for determining ion beam damage

This is the author's peer reviewed, accepted manuscript. However, the online version of record will be different from this version once it has been copyedited and typeset.

PLEASE CITE THIS ARTICLE AS DOI: 10.1063/1.50161681

can be summarized as: 1) Rutherford backscattering (RBS), 2) extended X-ray absorption fine structure (EXAFS) in synchrotrons, 3) atom probe tomography (APT) and 4) analytical transmission electron microscopy (ATEM). Compared to APT and ATEM, the probes of RBS and EXAFS have relatively poor spatial resolution (~30 nm)<sup>28</sup> so that local fragments of atomic clustering at nanometer scale are difficult to resolve. APT offers atomic resolution in 3D, unfortunately, the preferential ionization of certain atomic species during laser induced desorption is still a challenge for measuring the local chemical constitution<sup>29</sup>. Similar issues have been addressed in ATEM, where the development of aberration correctors has provided a possibility to probe chemical fluctuations at the nanometer scale, for example, in combining energy dispersive X-ray spectroscopy (EDXS) or electron energy-loss spectroscopy (EELS) with high-angle annular dark field imaging (HAADF), so ion irradiation induced structural and chemical modifications can be simultaneously studied at near-atomic scale. However, both HAADF and EDXS have little sensitivity to the type of chemical bonding, creating an obstacle for a direct understanding of ion/matter interaction. For core loss EELS, energy loss near-edge structure (ELNES) can directly probe the chemical constitution at nanometer scale, however, the energy range is usually limited to below 3 keV, so K-edges of heavy elements (such as Ga or In) cannot be easily accessed and studies are restricted to L- or M-edges.

Therefore, in this work, we investigate the cascade damage of Ga<sup>+</sup> ions in compound materials by using monochromated valence electron energy-loss (VEEL) spectroscopy, where the formation of chemical bonds in nano-precipitates can be evaluated at the nanoscale based on plasmon losses. A description of metal ion clustering during interstitial/vacancy annihilation must involve an understanding of preferential bond formation. We show that for Ga<sup>+</sup> ion implanted Al<sub>2</sub>O<sub>3</sub>, the importance of fast Frenkel pair recombination in Al<sub>2</sub>O<sub>3</sub> and Al-O bond formation can limit the occupation of Al sites with Ga<sup>+</sup> ions, leading to the precipitation of metallic Ga clusters. For Ga implantation into InP, although recoiled In and P atom display

short range recombination rates of vacancies/interstitials, the high Ga-P bond strength allows the formation of an InGaP ternary alloy. Finally, in case of ion cascades in InGaAs, heterogeneous distribution of interstitials and vacancies can lead to long-range recombination. The strong In-As and Ga-As bonds prevent In incorporation, resulting in the precipitation of In nano-clusters. The ion-solid interaction mechanisms in Al<sub>2</sub>O<sub>3</sub>, InP and InGaAs are proven to be independent of accelerating voltage, Ga<sup>+</sup> ion dose or dose rate.

A 500 nm InGaAs thin film layer on a 6 inch InP (001) substrate and commercial single-crystalline  $\alpha$ -Al<sub>2</sub>O<sub>3</sub> were purchased from Epihouse Optoelectronics Co., Ltd and Suzhou Crystal Silicon Electronic & Technology Co., Ltd, respectively. The Ga<sup>+</sup> ion damaged TEM specimens were prepared in a Thermo-Fisher Helios 600i equipped with a focused Ga<sup>+</sup> ion beam (FIB) system. The 30 kV Ga<sup>+</sup> ion beam current was used to extract a 1.5  $\mu$ m thick lamella from the top of the bulk sample with a beam current of ~2.5 nA. A beam diameter of ~10 nm was used for all experiments. Specimens were further thinned by 30 kV Ga<sup>+</sup> ion beams under an incident angle of 2°, where a beam current of 39 pA was used to mill the sample down to 200 nm.

An electron transparent region (~100 nm in thickness, estimated by VEELS in Fig. S1) was then produced by a 2 kV Ga<sup>+</sup> ion beam under an incident angle of 2° with a beam current of 23 pA, which enhances the ion implantation damage compared to conventional FIB polishing at ~9 pA. The details of all samples prepared for studying the dose, dose rate and accelerating voltage effects on Ga implantation can be found in the supplementary documents. Analytical transmission electron microscopy (TEM) was carried out on a Thermo-Fisher Titan Themis G2 double aberration corrected transmission electron microscope operated at 60 kV. The microscope is equipped with a monochromator and Gatan Quantum ER965 EELS system that allows an energy resolution of ~150 meV. The energy dispersive X-ray (EDX) elemental maps were recorded from Super-X silicon drift detectors, where the energy resolution and collection angle were nominally 136 eV and 0.9 srad, respectively.

This is the author's peer reviewed, accepted manuscript. However, the online version of record will be different from this version once it has been copyedited and typeset.

PLEASE CITE THIS ARTICLE AS DOI: 10.1063/5.0161681

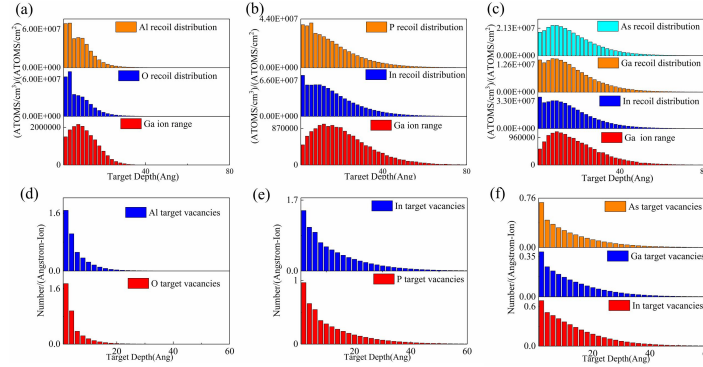


Fig. 1 Simulations of the depth distribution of recoiled atoms and Ga<sup>+</sup> ions for a) Al<sub>2</sub>O<sub>3</sub>, b) InP, c) InGaAs and of vacancies in d) Al<sub>2</sub>O<sub>3</sub>, e) InP and f) InGaAs.

To determine whether high energies (30 keV) are needed for creating major Ga<sup>+</sup> damage or whether low energies (2 keV) will suffice, three groups of reference specimens were prepared by 30 kV and 2 kV Ga<sup>+</sup> ion beams under same dose and dose rate, as shown in Fig. S2. A similar density of nanoclusters is observed in as-implanted samples prepared at 30 kV and with a subsequent polishing at 2 kV (Fig. S2 (b), (f) and (j)) and samples produced at 2 kV only (Fig. S2 (a), (e) and (i)), indicating significant damage already occurs at 2 kV. Therefore, the calculations of target atom recoil and vacancy depth distributions in Fig. 1 were performed by Monte Carlo simulation based on Stopping and Range of Ions in Materials (SRIM)<sup>30</sup> for an incident energy of 2 kV Ga<sup>+</sup> ions and an incidence angle of 2°, which correlates with the experimental FIB set-up. With respect to the mechanism of interstitial/vacancy annihilation we need to understand the interstitial/vacancy distribution. For distribution of interstitials/vacancies at similar depth (called homogenous distribution), the short-range interaction is expected to be dominated by recombination of Frenkel pairs, while the distribution of interstitials/vacancies at different depths (called heterogeneous distribution) could lead to long-range interstitial/vacancy annihilation. In case of Al<sub>2</sub>O<sub>3</sub> irradiated by Ga<sup>+</sup> ions (Fig. 1(a,d)), the shallow Al and O recoil atoms/vacancy distributions allow the interstitial/vacancy annihilation to be dominated by Frenkel pair recombination near the surface. Regarding Al vacancies occupied by Ga<sup>+</sup> ions, as the maximum Ga<sup>+</sup> ion range is found ~15 Å underneath the sputtered surface, the long-range interstitial/vacancy annihilation rate ( $R$ ) can be calculated from the heterogeneous distribution of Al

vacancies and Ga<sup>+</sup> ions from eq (1)<sup>24</sup>.

$$R = \sqrt[3]{3\Omega\sqrt{\pi}/A} \left( \frac{k_g \sqrt{x^2 D_g C_g}}{\Omega} \right) \quad (1)$$

where  $\Omega$  is the atomic volume,  $k_g$  the sink strength of the vacancy cluster,  $x$  the size of the vacancy cluster,  $D_g$  the diffusion coefficient of the interstitial/vacancy, and  $C_g$  the concentration of interstitial/vacancy. As the concentration of Al recoil atoms at 15 Å below the surface is approximately one order of magnitude larger than the maximum concentration of Ga<sup>+</sup> ions in Fig. 1(a), and the atomic volumes of Ga (11.8 cm<sup>3</sup>/mol) and Al (10 cm<sup>3</sup>/mol) are similar, the number of vacancy clusters captured by Al recoil atoms is approximately 23 times higher than that of Ga<sup>+</sup> ions. The preferential occupation of vacancy sites by Al recoil atoms will leave the Ga<sup>+</sup> ions clustered in Al<sub>2</sub>O<sub>3</sub>.

In InP, the recoil atoms and vacancies also exhibit a high distribution near the sputtered surface but range deeper into the crystal, allowing the In and P interstitial/vacancy annihilation to be dominated by Frenkel pair recombination. The recoiled In atom concentration at 15 Å below the surface is nearly two orders of magnitude higher than the maximum concentration of Ga<sup>+</sup> ions, so In recoil atoms will preferentially occupy the vacancy clusters ( $R_{In}$  is 26 times higher than  $R_{Ga}$ ), while the Ga<sup>+</sup> ions can penetrate even further and be incorporated into the lattice at larger depths. Finally, for InGaAs in Fig. 1(c,f), using the atomic volumes of In (15.7 cm<sup>3</sup>/mol), Ga (11.8 cm<sup>3</sup>/mol) and As (13.1 cm<sup>3</sup>/mol) as well as their corresponding interstitial concentrations according to eq. (1), the In interstitial/vacancy consumption rate is approximately 2.0 and 1.4 times higher than that of Ga and As, respectively, which could lead to a clustering

This is the author's peer reviewed, accepted manuscript. However, the online version of record will be different from this version once it has been copyedited and typeset.  
 PLEASE CITE THIS ARTICLE AS DOI: 10.1063/1.50161681

of In atoms in InGaAs of high In content.

Combining the HAADF images with EDX spectroscopy in Fig. S3, the Ga implantation damage in  $Al_2O_3$ , InP and InGaAs seems to agree with predictions from Monte Carlo simulations, where Ga is observed in  $Al_2O_3$  and In rich clusters in InP and in InGaAs, respectively.

However, dose rate effects are excluded in SRIM simulations where the influence of simultaneous ion arrival events cannot be modelled. High ion beam currents could change the ion range and the distributions of interstitials and vacancies

in FIB implantation compared to commercial broad ion beam systems<sup>31</sup>. Besides, lattice damage due to  $Ga^+$  ion implantation has been shown to be dose related in silicon, which was explained by the low solubility of Ga in Si.<sup>32</sup>

The nanoclusters observed by HAADF and EDXS in Figs. 2-4 could be either electron/ion irradiation induced metallic gallium/indium clusters<sup>33,34</sup> or locally In rich semiconductor compounds<sup>35</sup> produced by phase separation into indium depleted and indium rich alloys, leaving the cascade/sub-cascade induced interstitial/vacancy annihilation elusive.

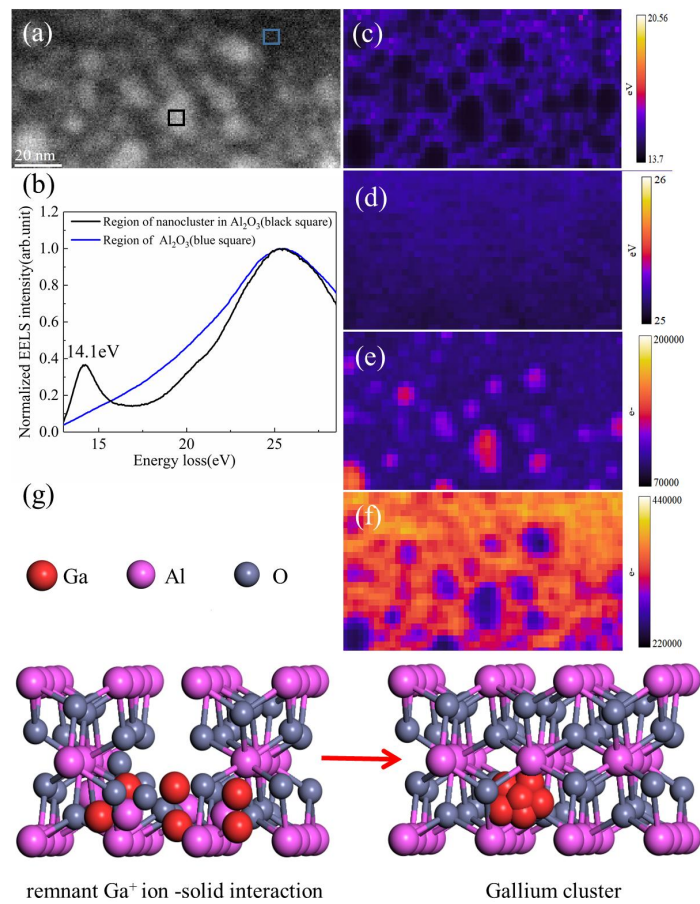


Fig.2 (a) HAADF of Ga implantation into  $Al_2O_3$ . (b) EELS spectra of reference and ion damaged regions in  $Al_2O_3$ . (c-f) The plasmon energy maps extracted correspond to a mixture of Ga and  $Al_2O_3$ . (g) Schematic diagram of interstitial/vacancy production and annihilation in  $Al_2O_3$ .

This is the author's peer reviewed, accepted manuscript. However, the online version of record will be different from this version once it has been copyedited and typeset.

PLEASE CITE THIS ARTICLE AS DOI: 10.1063/5.0161681

To investigate the local chemical bonding of the ion induced atomic clusters, plasmon energy loss spectroscopy is an ideal approach for analyzing local chemical constitution in ternary III-V semiconductors<sup>29,35,36</sup>. According to free electron approximation<sup>37</sup>, the frequency dependent plasmon energy is given by<sup>38</sup>

$$E_{pp} = \hbar\omega_p = \hbar \sqrt{\frac{NQ^2}{\epsilon_0 m_0}} \quad (2)$$

where  $E_{pp}$  is the free electron plasmon energy in EELS spectrum,  $\omega_p$  the plasmon frequency,  $\hbar$  the reduced Planck constant,  $N$  the number of valence electrons per unit cell,  $Q$  the elementary charge,  $V$  the volume of unit cell corresponding to doping concentration,  $m_0$  the electron mass, and  $\epsilon_0$  the permittivity of free space. Many metals and narrow bandgap semiconductors (GaAs, InAs and InP etc.) have relatively sharp plasmon peaks near the value predicted by this model. For ternary InGaAs, if the In rich nanoclusters observed were due to a high In content ternary alloy, the valence electron density could be expected to approach the density of valence electrons in InAs due to the expansion of unit cell volume, resulting in a plasmon energy between its binary alloys (GaAs: 15.5 eV<sup>39</sup> InAs: 14.1 eV<sup>40</sup>), while in case of precipitation of metallic In clusters (In bulk plasmon: 11.5 eV<sup>41</sup>) in InGaAs, two plasmon peaks would be expected to emerge in VEELS due to the different numbers of valence electrons per unit cell between metallic In and InGaAs. In contrast to ternary InGaAs, if an InGaP ternary alloy were formed due to Ga<sup>+</sup> injected into InP, the decrease of unit cell volume would increase the valence electron density, which could result in a blue shift of InP plasmon energy, while for Ga clusters precipitated in InP, similar to metallic Ga clusters in Al<sub>2</sub>O<sub>3</sub>, two individual plasmon peaks would be expected. For a wide bandgap binary alloy such as Al<sub>2</sub>O<sub>3</sub>, a plasmon excitation should involve the consideration of a bound oscillation near  $E_g$  (bandgap energy), i.e. a modified semi-free electron model that could lead to a blue shift of plasmon peak energy towards higher energy

( $E_p = \sqrt{E_p^2 + E_g^2}$ )<sup>38</sup>. For Ga<sup>+</sup> ion implanted Al<sub>2</sub>O<sub>3</sub>, if the Al site were occupied by a Ga atom instead, the decrease of bandgap and slight expansion of lattice volume would contribute to a plasmon peak shift towards lower energy (red shift). However, if the Ga rich area is dominated by metallic Ga, the wide bandgap of Al<sub>2</sub>O<sub>3</sub> (~8.7 eV)<sup>42</sup> implies the  $E_p$  of Al<sub>2</sub>O<sub>3</sub> is expected to be significantly larger than  $E_p$  of Ga, therefore, the individual plasmon peaks of Ga and Al<sub>2</sub>O<sub>3</sub> could be easily resolved in

VEELS even without a monochromator. Based on the principle of plasmon loss spectroscopy, VEEL spectrum imaging was performed to determine the chemical constitution of nanoclusters in Al<sub>2</sub>O<sub>3</sub> (Fig. 2). By extracting the spectrum (Fig. 2(b)) from a single nanocluster in Fig. 2(a) (black square area), an additional plasmon peak was observed at 14.1 eV, which correlates well with the plasmon energy of metallic Ga<sup>43</sup>. The Ga and Al<sub>2</sub>O<sub>3</sub> plasmon peaks can be modelled by multiple linear least-squares (MLLS) fitting as Lorentzian functions<sup>44</sup>. Maps of plasmon energy with their corresponding intensities are shown in Fig. 2(e-f). As can be seen in Fig. 2(e) and (f) (fitting energy window 13.8 eV-14.4 eV), the intensive metallic Ga plasmon resonance at 14.1±0.1 eV is only observed where nanoclusters are, indicating the nanoclusters are metallic Ga. No evidence of an Al-Ga alloy can be observed, once the energy uncertainty (±0.15 eV) is considered. In the plasmon energy map of Al<sub>2</sub>O<sub>3</sub> (Fig. 2(d)), of note, the structure of nano-precipitates has totally disappeared within the plasmon energy map, confirming pure Al<sub>2</sub>O<sub>3</sub> in the field of view. Only a relatively weak Al<sub>2</sub>O<sub>3</sub> plasmon intensity in Fig. 2(f) (fitting energy window 25.3 eV-25.9 eV) can be found in the regions with nano-precipitates, in agreement with Ga nanoclusters within an Al<sub>2</sub>O<sub>3</sub> matrix. The results are essentially consistent with the prediction of Ga implantation into Al<sub>2</sub>O<sub>3</sub> excluding any chemical bond formation. To reveal the physics behind the interaction between Ga<sup>+</sup> ion and Al<sub>2</sub>O<sub>3</sub>, the integral of crystal orbital Hamilton population (icohp) method<sup>45</sup> is adopted to investigate the bond formation between Al-O and Ga-O (Fig. S4), where the resultant integral intensity is summarized in Table 1. For crystal orbital Hamilton population (icohp), we have adopted the lobster simulation package, which is based on the VASP simulation code, and the calculated energies reported here are the overall integrals of all s,p,d states, including bonding as well as anti-bonding states. As can be seen in Table 1, the integral of crystal orbital Hamilton population (icohp) intensity of Al<sub>2</sub>O<sub>3</sub> (39 eV) is slightly larger than that of Ga<sub>2</sub>O<sub>3</sub> (34.9 eV), indicating preferential formation of Al-O bonds. Therefore, due to the superior rate of interstitial/vacancy consumption and dominance of Al-O bond formation in Al<sub>2</sub>O<sub>3</sub>, the limited recombination of Ga<sup>+</sup> ions with Al vacancies leads to precipitation of metallic Ga clusters. To support our analysis, the effects of Ga<sup>+</sup> ion accelerating voltage, dose and dose rate on Al<sub>2</sub>O<sub>3</sub> have also been investigated (Fig. S2, Fig. S6 and Fig. S7). As shown in Fig. S2 and Fig. S6, higher accelerating voltage and higher dose would enhance the structural damage in Al<sub>2</sub>O<sub>3</sub>.

This is the author's peer reviewed, accepted manuscript. However, the online version of record will be different from this version once it has been copyedited and typeset.

PLEASE CITE THIS ARTICLE AS DOI: 10.1063/1.50161681

However, the chemical constitution of nanoclusters remains metallic Ga independent of the ion accelerating voltage (Fig. S2 (d)) or dose (Fig. S6 (d)). For higher dose rate, the nanoclusters appear brighter and the Ga plasmon intensity increases, which can be attributed to the rapid amorphization of the ion bombarded surface that prohibits an effective Ga<sup>+</sup> ion channeling in the crystalline regions of the specimen<sup>31,46,47</sup>. However, the mechanism of metallic Ga nano-precipitates forming is the same,

irrelevant of the dose rate. A schematic diagram of Ga<sup>+</sup> ion implantation in Al<sub>2</sub>O<sub>3</sub> is shown in Fig. 2(g).

Table 1 icohp calculation of Al-O, Ga-O, In-P, Ga-P, Ga-As and In-As

icohp(eV)	bonds					
	Al-O	Ga-O	In-P	Ga-P	Ga-As	In-As
	39	34.9	0.1	24.2	33.2	38.3

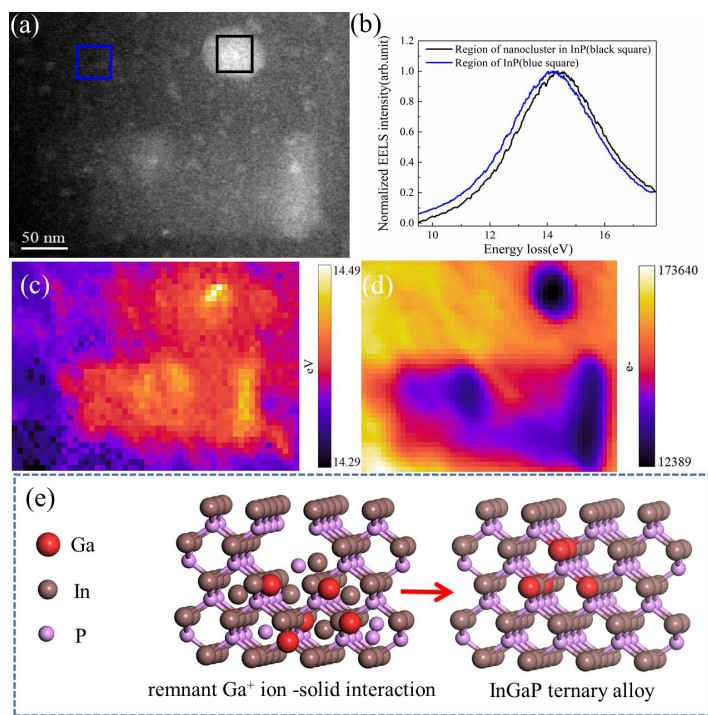


Fig.3 (a) HAADF of Ga implantation into InP. (b) VELS spectra of reference and ion damaged regions in InP. (c-d) The plasmon energy distribution maps extracted are in agreement with InGaP. (e) Schematic diagram of interstitial/vacancy production and annihilation in InP, leading to ternary InGaP.

This is the author's peer reviewed, accepted manuscript. However, the online version of record will be different from this version once it has been copyedited and typeset.

PLEASE CITE THIS ARTICLE AS DOI: 10.1063/5.0161681

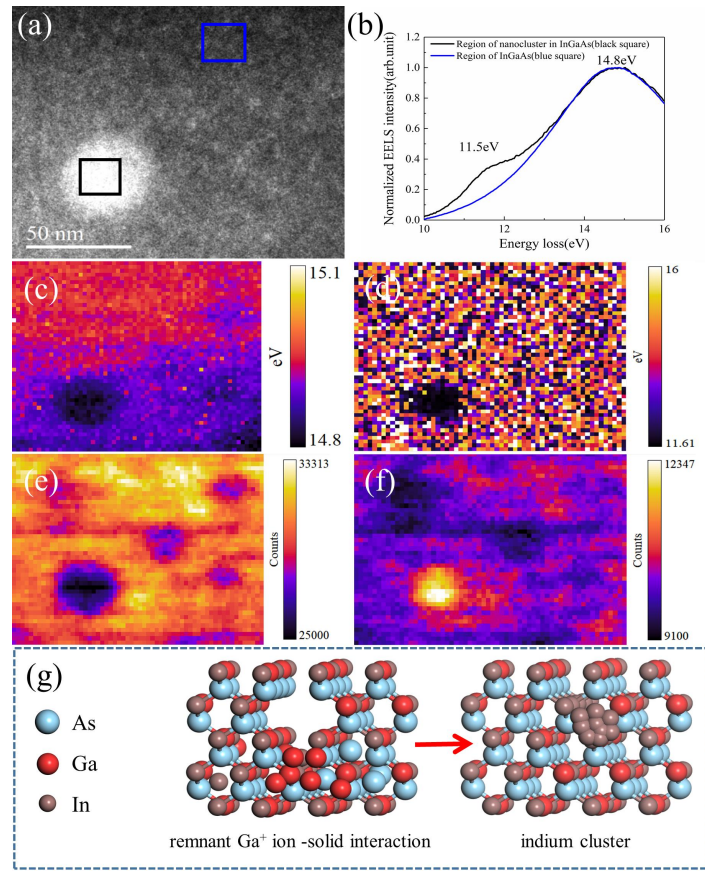


Fig. 4 (a) HAADF of Ga<sup>+</sup> ion damaged region in InGaAs. (b) VEEEL spectra of reference (blue square region) and nano-precipitates (black square region) in InGaAs. (c-f) Plasmon energy maps of InGaAs and In. (g) Schematic diagram of metallic In segregation under Ga<sup>+</sup> ion irradiation.

Comparing clusters in Ga implanted InP (black square region in Fig. 3(a) and black curve in Fig. 3(b)) with InP bulk plasmon spectrum (blue square region in Fig. 3(a) and blue curve in Fig. 3(b)), a small but noticeable blue shift of the plasmon peak and an absence of metallic Ga plasmon resonances is observed in the region of nanoclusters (Fig. 3(c)). Also, a lowered InP plasmon intensity (Fig. 3(d) fitting energy window: 14.0 – 14.6 eV) was found in the region of nano-precipitates, suggesting the formation of a ternary InGaP. According to the SRIM simulation, the injected Ga<sup>+</sup> ions are expected to cluster in InP, which seems to contradict our experimental observation.

Nevertheless, according to Table 1, the Ga atoms prefer to bond with P atoms much stronger than In atoms do (icohp intensity of GaP = 24.2 eV versus 0.1 eV for InP), resulting in a likely replacement of some In by Ga atoms within the sphalerite lattice, leading to the formation of a ternary InGaP alloy. Similar to Al<sub>2</sub>O<sub>3</sub>, the dependence of accelerating voltage, dose and dose rate of Ga<sup>+</sup> ion-InP interaction has been investigated. As can be seen in Fig. S2, Fig. S6 and Fig. S7, the change of Ga<sup>+</sup> ion accelerating voltage, dose or dose rate will only give rise to the formation of InGaP ternary alloy. Therefore, the mechanism of interstitial/vacancy annihilation in InP (Fig. 3 (e)) is proven to be

This is the author's peer reviewed, accepted manuscript. However, the online version of record will be different from this version once it has been copyedited and typeset.

PLEASE CITE THIS ARTICLE AS DOI: 10.1063/5.0161681

independent of ion dose and dose rate.

Finally, plasmon loss spectroscopy was used to analyze the chemical constitution of nano-precipitates in Ga-implanted InGaAs. As the indium containing semiconductor suffers from electron irradiation damage for beam currents above  $\sim 100$  pA at 200 kV accelerating voltage<sup>48</sup>, therefore, the optimization of probe dose rate as well as the accelerating voltage is of importance for minimizing the electron irradiation damage. In our experimental set-up, the beam current of a monochromated 60 kV electron probe approached  $\sim 20$  pA within a 2 nm pixel size. Rastering the InGaAs based quantum well with this convergent beam for 30 min, any electron beam damage remains invisible (supplementary data in Fig. S5). Therefore, the optimized accelerating voltage and electron dose level ( $10^8$  /cm<sup>2</sup>) of the probe are proven ideal for recording InGaAs VEEL spectrum images. The large nanoparticle in Fig. 4(a) (region of black square) displays a plasmon shoulder around  $\sim 11.5$  eV (Fig. 4(b)), which agrees with the plasmon energy of metallic In<sup>39</sup>. By modelling both plasmon peaks with MLLS fitting routines, the plasmon energy and peak intensity maps of InGaAs in Figs. 4(c-f) agree with In-rich InGaAs around the nano-precipitate, which correlates well with the theoretical prediction. According to Fig. 4 (e: InGaAs fitting energy window 14.5 – 15.1 eV, f: In fitting energy window: 11.2 – 11.8 eV), the intensive In plasmon resonance of the nanocluster is identified as being due to metallic In, indicating metallic In segregation within In rich InGaAs. Considering the relative bond strengths of In-As (38.3 eV) and Ga-As (33.2 eV) in Table 1, an entire occupation of vacancies by In atoms would be unlikely, leading to oversaturated In interstitials being precipitated near the high In content InGaAs region. According to HAADF and VEEL spectra in Fig. S2, Fig. S6 and Fig. S7, variation of the ion accelerating voltage, dose or dose rate does not change the chemical constitution of the nano-precipitates, indicating the implanted Ga<sup>+</sup> ion induced In segregation is independent of dose and dose rate. Therefore, the schematic diagram of Ga<sup>+</sup> ion induced In segregation in InGaAs layer can be proposed as shown in Fig. 4(g).

In summary, we have explained different cluster formation mechanisms in Ga<sup>+</sup> ion implanted materials based on an annihilation of interstitial/vacancy complexes during heavy ion irradiation and preferential bond formation. For Ga<sup>+</sup> ion cascades in Al<sub>2</sub>O<sub>3</sub>, the superior vacancy capturing rate of Al and high bond strength of Al-O are responsible for producing metallic Ga clusters. For Ga sputtered InP, the preferential Ga-P bonding can

prompt Ga incorporation into the lattice, enabling the local formation of an InGaP ternary alloy. Finally, in case of Ga<sup>+</sup> ion implanted InGaAs, In recoil atoms prefer to occupy vacancies and excess In interstitials are expected to form In-rich nano-precipitates. These remnant ion-solid interaction mechanisms are proven to be independent of accelerating voltage, dose and dose rate of Ga<sup>+</sup> ions. Our finding yields guidance for investigating ion induced damage in compound materials, combining ion/matter interaction theory with VEELS experiments probing the local plasmons formed.

#### Supplementary Material

**S1:** EELS for thickness measurement for Al<sub>2</sub>O<sub>3</sub>, InP and InGaAs, respectively. **S2:** effects of different voltages on Al<sub>2</sub>O<sub>3</sub>, InP and InGaAs. **S3:** HAADF and EDX spectrum of Al<sub>2</sub>O<sub>3</sub>, InP and InGaAs, respectively. **S4:** Crystal orbital Hamilton population (COHP) calculation of Al-O, Ga-O, In-P, Ga-P, Ga-As and In-As. **S5:** HAADF, plasmon maps of chemical constitution and EELS. **S6-S7:** Effects of different doses and dose rates on Al<sub>2</sub>O<sub>3</sub>, InP and InGaAs.

This work was supported by the National Natural Science Foundation of China (61975075), the Department of Science and Technology of Sichuan Province under grant numbers (2023YFH0054), the Technology and Innovation Commission of the Shenzhen Municipality (JCYJ20190809142019365). The authors acknowledge the assistance of SUSTech Core Research Facilities and the help of Dr. DongSheng He at Pico Center for the aberration corrected TEM experiments. The Strategic Cooperation Projects were fostered by Zigong government and Sichuan University (No. 2021CDZG-22) and the Institutional Foundation of Institute of Chemical Materials, China Academy of Engineering Physics (No. 2021SJYBXM0217). Zhenyu Ma and Xiaoyi Wang are sincerely acknowledging partial financial support from Dr Jinpeng Yu and Rong Wen in Sichuan Yuqian Technology Co., Ltd

Author declarations: The authors have no conflicts to disclose.

Data availability: the data that support the findings of this study are available from the corresponding authors upon reasonable request.

This is the author's peer reviewed, accepted manuscript. However, the online version of record will be different from this version once it has been copyedited and typeset.

PLEASE CITE THIS ARTICLE AS DOI: 10.1063/1.50161681

#### Reference

- <sup>1</sup>A. A. Haasz, M. Poon and J. W. Davis, The effect of ion damage on deuterium trapping in tungsten. *J. Nucl. Mater.* 266-269, 520-525 (1999).
- <sup>2</sup>F. W. Sexton, D. M. Fleetwood, M. R. Shaneyfelt, P. E. Dodd, G. L. Hash, L. P. Schanwald, R. A. Loomer, K. S. Krisk, M. L. Green and B. E. Weir, Precursor ion damage and angular dependence of single event gate rupture in thin oxides. *IEEE T. Nucl. Sci.* 45, 2509-2518 (1998)
- <sup>3</sup>L. Nan, E. G. Fu, H. Wang, J. J. Carter, L. Shao, S. A. Maloy, A. Misra and X. Zhang, He ion irradiation damage in Fe/W nanolayer films. *J. Nucl. Mater.* 389, 233-238 (2009).
- <sup>4</sup>E. Wendler, K. Gartner and W. Wesch, Comparison of ion-induced damage formation in and MgO. *Nucl. Mater.* 266,2872-2876 (2008).
- <sup>5</sup>S. Xu, Z. Yao and M. L. Jenkins, TEM characterisation of heavy-ion irradiation damage in FeCr alloys. *J. Nucl. Mater.* 386,161-164 (2009)
- <sup>6</sup>J. R. Conrad, Plasma source ion-implantation technique for surface modification of materials. *J. Appl. Phys.* 62,4591-4596 (1987).
- <sup>7</sup>A. Ghicov, J. M. Macak, H. Tsuchiya, J. Kunze, V. Haeublein, L. Frey and P. Schmuki, Ion Implantation and Annealing for an Efficient N-Doping of TiO<sub>2</sub> Nanotubes. *Nano Lett.* 6,1080-1082 (2006).
- <sup>8</sup>A. Meldrum, F. R. Jr. Haglund, L. A. B. And and C. W. White, Nanocomposite Materials Formed by Ion Implantation. *Adv. Mater.* 13, 1431-1444 (2001).
- <sup>9</sup>M. A. De. Crosta, Effect of ion implantation and silanization on the corrosion and cathodic delamination resistances of mild steel. *Pediatr. Allergy Immunol.* 5, 196-205 (2004).
- <sup>10</sup>M. Anpo, Y. Ichihashi, M. Takeuchi and H. Yamashita, Design of unique TiO<sub>2</sub> photocatalysts by an advanced metal ion-implantation method and photocatalytic reactions under visible light irradiation. *Res. Chem. Intermediate* 24,143-149 (1998).
- <sup>11</sup>S. Zhou, K. Potzger, J. V. Borany, R. Groetzschel and J. Fassbender, Crystallographically oriented Co and Ni nanocrystals inside ZnO formed by ion implantation and post-annealing. *Phys. Rev. B* 77, 35209-35209 (2008).
- <sup>12</sup>S. M. S. Privitera, A. M. Mio, E. Smecca and A. Alberti, Structural and electronic transitions in Ge<sub>2</sub>Sb<sub>2</sub>Te<sub>5</sub> induced by ion irradiation damage. *Phys. Rev. B* 94,094103 (2016).
- <sup>13</sup>J. A. Farmer, C. T. Campbell, L. Xu and G. Henkelman, Defect sites and their distributions on MgO (100) by Li and Ca adsorption calorimetry. *J. Am. Chem. Soc.* 131, 3098-103 (2009).
- <sup>14</sup>A. A. Correa, K. Jorge, E. Artacho, S. P. Daniel and A. Caro, Nonadiabatic forces in ion-solid interactions: The initial stages of radiation damage. *Phys. Rev. Lett.* 109, 069901 (2012).
- <sup>15</sup>D. A. Young, Molecular dynamics simulation of swift ion damage in lithium fluoride. *Nucl. Instrum. Meth. B.* 225, 231-240 (2004).
- <sup>16</sup>D. Humbird and D. B. Graves, Ion-induced damage and annealing of silicon. Molecular dynamics simulations. *Pure Appl. Chem.* 74, 419-422 (2002).
- <sup>17</sup>A. K. Revelly, G. Monpara, I. Samajdar, K. V. Krishna, R. ManiTevari, D. Srivastava, G. K. Dey and A. S. Panwar, Effect of Gallium ion damage on poly-crystalline Zirconium: Direct experimental observations and molecular dynamics simulations. *J. Nucl. Mater.* 467 155-164 (2015).
- <sup>18</sup>A. M. Mazzone, Monte Carlo methods in defects migration—Spontaneous annealing of damage induced by ion implantation. *IEEE T. Electron Dev.* 32, 1925-1929 (1985).
- <sup>19</sup>N. Peng, C. Jeynes, R. Webb, I. Chakarov and M. Blamire, Monte Carlo simulations of masked ion beam irradiation damage profiles in YBa<sub>2</sub>Cu<sub>3</sub>O<sub>7</sub>-delta thin films. *Nucl. Instrum. Meth. B* 178, 242-246 (2001)
- <sup>20</sup>F. Gao and W. J. Weber, Recovery of close Frenkel pairs produced by low energy recoils in SiC. *J. Appl. Phys.* 94, 4348-4356 (2003).
- <sup>21</sup>N. Pannier, A. Guglielmetti, L. V. Brutzel and A. Chartier, Molecular dynamics study of Frenkel pair recombinations in fluorite type compounds. *Nucl. Instrum. Meth. B* 267, 3118-3121 (2009).
- <sup>22</sup>R. E. Stoller, G. R. Odette and B. D. Wirth, Primary damage formation in bcc iron. *J. Nucl. Mater.* 251, 49-60 (1997).
- <sup>23</sup>X. M. Duan and C. Stampfl, Vacancies and interstitials in indium nitride: Vacancy clustering and molecular bondlike formation from first principles. *Phys. Rev. B* 79, 174202 (2009).
- <sup>24</sup>B. N. Singh, S. I. Golubov, H. Trinkaus, A. Serra, Y. N. Osetsyk and A.V. Barashev, Aspects of microstructure evolution under cascade damage conditions. *J. Nucl. Mater.* 251, 107-122 (1997).
- <sup>25</sup>H. Hofäss and K. Zhang, Surfactant sputtering. *Appl. Phys. A*, 92, 517-524 (2008).
- <sup>26</sup>H. Hofäss, K. Zhang and A. Pape, The role of phase separation for self-organized surface pattern formation by ion beam erosion and metal atom co-deposition. *Appl. Phys. A*, 111, 653-664 (2013).
- <sup>27</sup>Y. J. Xu, K. Zhang, C. Brüsewitz, X. Wu and H. Christian, Investigation of the effect of low energy ion beam irradiation on mono-layer graphene. *AIP Adv.* 3, 72120-72120 (2013).
- <sup>28</sup>S. Peth, R. Horn, F. Beckmann, T. Donath, J. Fischer and A.J.M. Smucker, Three-Dimensional Quantification of Intra-Aggregate Pore-Space Features using Synchrotron-Radiation-Based Microtomography. *Soil Sci. Soc. Am. J.*, 72, 897-907 (2008).
- <sup>29</sup>X. Y. Wang, Characterization of InGaN Thin Films and Nanowires by Analytical Transmission Electron Microscopy. PhD thesis, University of Sheffield (2018).
- <sup>30</sup>J. F. Ziegler, SRIM-2003. *Nucl. Instrum. Meth. B*, 219, 1027-1036 (2004).
- <sup>31</sup>G. P. S. Balasubramanian and R. Hull, Mechanisms of Focused Ion Beam Implantation Damage and Recovery in Si. *J. Electron. Mater.* 45,

This is the author's peer reviewed, accepted manuscript. However, the online version of record will be different from this version once it has been copyedited and typeset.

PLEASE CITE THIS ARTICLE AS DOI: 10.1063/1.50161681

3236-3243 (2016).

<sup>32</sup>G. P. S. Balasubramanian and R. Hull, Damage recovery of FIB modified Si for directed-assembly of semiconductor nanostructures. *J. Mater. Sci. Mater. Electron.* **26**, 1-8 (2015).

<sup>33</sup>H. Yamamoto and H. Asaoka, Formation of binary clusters by molecular ion irradiation. *Appl. Surf. Sci.*, **169**, 305-309 (2001).

<sup>34</sup>P. Kluth, B. Johannessen, G. Foran, D. Cookson, S. Kluth and M. Ridgway, Disorder and cluster formation during ion irradiation of Au nanoparticles in SiO<sub>2</sub>. *Phys. Rev. B*, **74**, 4202 (2006).

<sup>35</sup>T. Walther and X. Wang, Self-consistent method for quantifying indium content from X-ray spectra of thick compound semiconductor specimens in a transmission electron microscope. *J. Microsc.* **262**, 151-156 (2016).

<sup>36</sup>X. Wang, M.-P. Chauvat, P. Ruterana and T. Walther, Investigation of phase separation in InGaN alloys by plasmon loss spectroscopy in a TEM. *MRS Advances*, **1**:40, 2749-2756 (2016).

<sup>37</sup>J. M. Ziman, The T matrix, the K matrix, d bands and l-dependent pseudo-potentials in the theory of metals. *Proc. of the Physical Society*, **86**, 337 (1965).

<sup>38</sup>W. Zhan, V. Venkatachalapathy, T. Aarholt, A. Y. Kuznetsov and Y. Prytz, Band gap maps beyond the delocalization limit: correlation between optical band gaps and plasmon energies at the nanoscale. *Sci. Rep.*, **8**, 848 (2018).

<sup>39</sup>L. Bideux, D. Baca and B. Gruzza, Surface modification of GaAs during argon ionic cleaning and nitridation: EELS, EPES and XPS studies. *Surf. Sci.* **566**, 1158-1162 (2004).

<sup>40</sup>L. H. G. Tizei, T. Chiaramonte, M. A. Cotta and D. Ugarte, Characterization of interface abruptness and material properties in catalytically grown III - V nanowires: exploiting plasmon chemical shift. *Nanotechnology*, **21**, 295701 (2010).

<sup>41</sup>M. Bouslama, M. Ghamnia, B. Gruzza, F. Miloua and C. Jardin, AES and EELS analysis of the interaction between phosphorus and metallic indium. *J. Electr. Spectrosc.*, **68**, 377-382 (1994).

<sup>42</sup>P. Thompson, D. E. Cox and J. B. Hastings, Rietveld refinement of Debye-Scherrer synchrotron X-ray data from Al<sub>2</sub>O<sub>3</sub>. *J. Appl. Crystallogr.* **20**, 79-83 (1987).

<sup>43</sup>M. L. Mata, S. C. Gómez, F. Nucciarelli, J. L. Pau and S. I. Molina, High Spatial Resolution Mapping of Localized Surface Plasmon Resonances in Single Gallium Nanoparticles. *Small* **15**, e1902920 (2019).

<sup>44</sup>T. Walther, X. Y. Wang, V. C. Angadi, P. Ruterana, P. Longo and T. Aoki, Study of phase separation in an InGaN alloy by electron energy loss spectroscopy in an aberration corrected monochromated scanning transmission electron microscope. *J. Mater. Res.*, **32**, 983-995 (2017).

<sup>45</sup>V. Fung, Z. Wu and D. Jiang, New bonding model of radical adsorbate on lattice oxygen of perovskites. *J. Phys. Chem. Lett.*, **2018**, 9(21): 6321-6325.

<sup>46</sup>M. Tamura, S. Shukuri and M. M. Default, Focused ion beam gallium implantation into silicon. *Appl. Phys. A*, **39**, 183-190 (1986).

<sup>47</sup>H. J. Lezec, C. R. Musil, J. Melngailis, Dose - rate effects in focused - ion - beam implantation of Si into GaAs. *J. Vac. Sci. Technol. B*, **9**, 2709-2713 (1991).

<sup>48</sup>H. Ohyama, K. Kobayashi, J. Vanhellefont, E. Simoen, C. Claeys, K. Takakura, T. Hirao and S. Onoda, Induced lattice defects in InGaAs photodiodes by high-temperature electron irradiation. *Physica B*, **342**:337-340 (2003).

This is the author's peer reviewed, accepted manuscript. However, the online version of record will be different from this version once it has been copyedited and typeset.

**PLEASE CITE THIS ARTICLE AS DOI: 10.1063/5.0161681**

This is the author's peer reviewed, accepted manuscript. However, the online version of record will be different from this version once it has been copyedited and typeset.

**PLEASE CITE THIS ARTICLE AS DOI: 10.1063/5.0161681**

This is the author's peer reviewed, accepted manuscript. However, the online version of record will be different from this version once it has been copyedited and typeset.

**PLEASE CITE THIS ARTICLE AS DOI: 10.1063/5.0161681**

This is the author's peer reviewed, accepted manuscript. However, the online version of record will be different from this version once it has been copyedited and typeset.

**PLEASE CITE THIS ARTICLE AS DOI: 10.1063/5.0161681**